

A&A manuscript no.
(will be inserted by hand later)

Your thesaurus codes are:
06(02.18.7, 03.13.4, 08.14.1, 08.19.4, 02.05.1)

ASTRONOMY
AND
ASTROPHYSICS
23.8.2021

Neutrino transport in type II supernovae: Boltzmann solver vs. Monte Carlo method

Shoichi Yamada^{1,2 *}, Hans-Thomas Janka^{1**}, and Hideyuki Suzuki^{1,3***}

¹ Max-Planck-Institut für Astrophysik, Karl-Schwarzschild-Str. 1, Postfach 1523, D-85740 Garching, Germany

² Department of Physics, Graduate School of Science, The University of Tokyo, 7-3-1, Hongo, Bunkyo-ku, Tokyo 113, Japan

³ High Energy Accelerator Research Organization (KEK), Oho, Tsukuba, Ibaraki 305-0801, Japan

Received; accepted

Abstract. We have coded a Boltzmann solver based on a finite difference scheme (S_N method) aiming at calculations of neutrino transport in type II supernovae. Close comparison between the Boltzmann solver and a Monte Carlo transport code has been made for realistic atmospheres of post bounce core models under the assumption of a static background. We have also investigated in detail the dependence of the results on the numbers of radial, angular, and energy grid points and the way to discretize the spatial advection term which is used in the Boltzmann solver. A general relativistic calculation has been done for one of the models. We find overall good agreement between the two methods. This gives credibility to both methods which are based on completely different formulations. In particular, the number and energy fluxes and the mean energies of the neutrinos show remarkably good agreement, because these quantities are determined in a region where the angular distribution of the neutrinos is nearly isotropic and they are essentially frozen in later on. On the other hand, because of a relatively small number of angular grid points (which is inevitable due to limitations of the computation time) the Boltzmann solver tends to underestimate the flux factor and the Eddington factor outside the (mean) “neutrinosphere” where the angular distribution of the neutrinos becomes highly anisotropic. As a result, the neutrino number density is overestimated in this region. This fact suggests that one has to be cautious in applying the Boltzmann solver to a calculation of the neutrino heating in the hot-bubble region because it might tend to overestimate the local energy deposition rate. A comparison shows that this trend is opposite to the results obtained with a multi-group flux-limited diffusion approximation of neutrino transport, employing three different flux limiters, all of which lead to an underesti-

mation of the hot-bubble heating. The accuracy of the Boltzmann solver can be considerably improved by using a variable angular mesh to increase the angular resolution in the semi-transparent regime.

Key words: radiative transfer – methods: numerical – stars: neutron – supernovae: general – elementary particles: neutrinos

1. Introduction

Neutrino energy transfer to the matter adjacent to the nascent neutron star is supposed to trigger the explosion of a massive star ($M \gtrsim 8 M_\odot$) as a type II supernova. Since the energy released in neutrinos by the collapsed stellar iron core is more than 100 times larger than the kinetic energy of the explosion, only a small fraction of the neutrino energy is sufficient to expel the mantle and envelope of the progenitor star. Numerical simulations have demonstrated the viability of this neutrino-driven explosion mechanism (Wilson 1982; Bethe & Wilson 1985; Wilson et al. 1986) but the explosions turned out to be sensitive to the size of the neutrino luminosities and the neutrino spectra (Janka 1993; Janka & Müller 1993; Burrows & Goshy 1993) both of which determine the power of the neutrino energy transfer to the matter outside the average neutrinosphere. The rate of energy deposition per nucleon via the dominant processes of electron neutrino absorption on neutrons and electron antineutrino absorption on protons is given by:

$$Q_\nu^+ \approx 110 \cdot \frac{L_{\nu,52} \langle \epsilon_{\nu,15}^2 \rangle}{r_7^2 \langle \mu \rangle} \cdot \left\{ \frac{Y_n}{Y_p} \right\} \left[\frac{\text{MeV}}{\text{s} \cdot N} \right]. \quad (1)$$

Here $Y_n = n_n/n_b$ and $Y_p = n_p/n_b$ are the number fractions of free neutrons and protons, respectively; the normalization with the baryon density n_b indicates that the

Send offprint requests to: S. Yamada

* e-mail: shoichi@MPA-Garching.MPG.DE

** e-mail: thj@MPA-Garching.MPG.DE

*** e-mail: hideyuki.suzuki@kek.jp

rate per baryon is calculated in Eq. (1). $L_{\nu,52}$ denotes the luminosity of either ν_e or $\bar{\nu}_e$ in units of 10^{52} erg/s and r_7 is the radial position in 10^7 cm. The average of the squared neutrino energy, $\langle \epsilon_{\nu,15}^2 \rangle$, is measured in units of $(15 \text{ MeV})^2$ and enters through the energy dependence of the neutrino and antineutrino absorption cross sections. $\langle \mu \rangle$ is the angular dilution factor of the neutrino radiation field (the “flux factor”, which is equal to the mean value of the cosine of the angle of neutrino propagation relative to the radial direction) which varies between values much less than unity deep inside the protoneutron star atmosphere, about 0.25 around the neutrinosphere, and 1 for radially streaming neutrinos very far out. The factor $\langle \mu \rangle$ determines the local neutrino energy density according to the relation $E_\nu = L_\nu / (4\pi r^2 c \langle \mu \rangle)$ and thus enters the heating rate of Eq. (1). Only far away from the neutrino emitting star, $\langle \mu \rangle \rightarrow 1$, and E_ν dilutes like r^{-2} .

Although it was found in two-dimensional simulations that convective instabilities in the neutrino-heating region can help the explosion (Herant et al. 1994; Janka & Müller 1993, 1996; Burrows et al. 1995; Miller et al. 1993; Shimizu et al. 1994) by the exchange of hot gas from the heating layer with cold gas from the postshock region, the strength of this convective overturn and its importance for the explosion is still a matter of debate (Janka & Müller 1996, Mezzacappa et al. 1998, Lichtenstadt et al. 1998). In addition, it turns out that the development of an explosion remains sensitive to the neutrino luminosities and the mean spectral energies even if convective overturn lowers the required threshold values. This is the case because convective instabilities can develop sufficiently quickly only when the heating is fast and an unstable stratification builds up more quickly than the heated matter is advected from the postshock region through the gain radius (which is the radius separating neutrino cooling inside from neutrino heating outside) down onto the neutron star surface (Janka & Müller 1996, Janka & Keil 1998).

“Robust” neutrino-driven explosions might therefore require larger accretion luminosities (to be precise: a larger value of the product $L_\nu \langle \epsilon_\nu^2 \rangle$ in Eq. (1)) during the early post-bounce phase, or might call for enhanced neutrino emission from the core. The latter could be caused, for example, by convective neutrino transport within the nascent neutron star (Burrows 1987; Mayle & Wilson 1988; Wilson & Mayle 1988, 1993; Keil et al. 1996) or, alternatively, by a suppression of the neutrino opacities at nuclear densities through nucleon correlations (Sawyer 1989; Horowitz & Wehrberger 1991; Raffelt & Seckel 1995; Raffelt et al. 1996; Keil et al. 1995; Janka et al. 1996; Burrows & Sawyer 1998a,b; Reddy et al. 1998a), nucleon recoil and blocking (Schinder 1990) and/or nuclear interaction effects in the neutrino-nucleon interactions (Prakash et al. 1997; Reddy et al. 1997, 1998b), all of which have to date not been taken into account fully self-

consistently in supernova simulations. The diffusive propagation of neutrinos out from the very opaque inner core is determined by the value of the diffusion constant and thus sensitive to these effects.

Most of the current numerical treatments of neutrino transport, however, are deficient not only concerning their description of the extremely complex neutrino interactions in the dense nuclear plasma but also concerning their handling of the transition from diffusion to free streaming. While the core flux is fixed in the diffusive regime, the accretion luminosity as well as the spectra of the emitted neutrinos depend on the transport in the semitransparent layers around the sphere of last scattering. Since neutrino-matter interactions are strongly dependent on the neutrino energy, neutrinos with different energies interact with largely different rates and decouple in layers with different densities and temperatures. The spectral shape of the emergent neutrino flux is therefore different from the thermal spectrum at any particular point in the atmosphere. Even more, through the factor $\langle \mu \rangle$ in the denominator of Eq. (1) the energy deposition rate depends on the angular distribution of the neutrinos in the heating region. A quantitatively reliable description of these aspects requires the use of sophisticated transport algorithms which solve the Boltzmann equation instead of approximate methods like flux-limited diffusion techniques (Janka 1991a, 1992; Mezzacappa & Bruenn 1993a,b,c; Messer et al. 1998). The detection of electron antineutrinos from SN 1987A in the Kamiokande II (Hirata et al. 1987) and IMB laboratories (Bionta et al. 1987) and the construction of new, even larger neutrino experiments for future supernova neutrino measurements have raised additional interest in accurate predictions of the detectable neutrino signals from type II supernovae.

Neutrino transport in core collapse supernovae is a very complex problem and difficult to treat accurately even in the spherically symmetric case. Some of the major difficulties arise from the strong energy dependence of the neutrino interactions, the non-conservative and anisotropic nature of the scattering processes such as neutrino-electron scattering, the non-linearity of the reaction kernels through neutrino Fermi blocking, and the need to couple neutrino and antineutrino transport for the neutrino-pair reactions. Therefore various simplifications and approximations have been employed in numerical simulations of supernova explosions and neutron star formation. The so far most widely used approximation with a high degree of sophistication is the (multi-energy-group) flux-limited diffusion (MGFLD) (Bowers & Wilson 1982, Bruenn 1985, Myra et al. 1987, Suzuki 1990, Lichtenstadt et al. 1998) where a flux-limiting parameter is employed in the formulation of the neutrino flux to ensure a smooth interpolation between the diffusion regime (where the neutrinos are essentially isotropic) and the free streaming regime (where the neutrinos move ra-

dially outward). Although the limits are accurately reproduced, there is no guarantee that the intermediate regime is properly treated. Since in a quasi-stationary situation (e.g., for the cooling protoneutron star) the flux and the mean energy of the emitted neutrinos are determined in the diffusion regime, little change of these is found when the flux-limiter is varied (Suzuki 1990) or the transport equation is directly solved, e.g., by Monte Carlo calculations (Janka 1991a). This, however, is not true when the spectral form is considered, because the spectra are shaped in the semitransparent surface-near layers. Moreover, significant differences are also expected for problems where the local angular distribution is important in the region between the diffusion and free streaming limits. Due to the factor $\langle\mu\rangle$ appearing in Eq. (1) the hot-bubble heating is such a problem, neutrino-antineutrino pair annihilation is another problem of this kind. In fact, Monte Carlo simulations (Janka & Hillebrandt 1989a,b; Janka 1991a; Janka et al. 1992) have shown that all flux-limiters overestimate the anisotropy of the radiation field outside the neutrinosphere, i.e., $\langle\mu\rangle = 1$ is enforced too rapidly (see also Cernohorsky & Bludman 1994). This leads to an underestimation of the neutrino heating in the hot-bubble region between neutrinosphere and supernova shock (Eq. (1)), and sensitivity of the supernova dynamics to the employed flux-limiting scheme must be expected (Messer et al. 1998, Lichtenstadt et al. 1998).

Modifications of flux-limited diffusion have been suggested (Janka 1991a, 1992; Dgani & Janka 1992, Cernohorsky & Bludman 1994) by which considerable improvement can be achieved for spherically symmetric, static and time-independent backgrounds (Smit et al. 1997), but satisfactory performance for the general time-dependent and non-stationary case has not been demonstrated yet. Therefore the interest turns towards direct solutions of the Boltzmann equation for neutrino transport, also because the need to check the applicability of any approximation with more elaborate methods remains. Moreover, the rapid increase of the computer power and the wish to become independent of ad hoc constraints on generality or accuracy yield a motivation for the efforts of several groups (in particular Mezzacappa & Bruenn 1993a,b,c and Messer et al. 1998; more recently also Burrows 1997) to employ such Boltzmann solvers in neutrino-hydrodynamics calculations of supernova explosions.

There are different possibilities to solve the Boltzmann equation numerically, one of which is by straightforward discretization of spatial, angular, energy, and time variables and conversion of the differential equation into a finite difference equation which can then be solved for the values of the neutrino phase space distribution function at the discrete mesh points. Dependent on the number N of angular mesh points, this procedure is called S_N method. Since solving the equation is computationally very expensive, there are limitations to the resolution in angle and

energy space. Therefore tests need to be done whether a chosen (and affordable) number of energy and angle grid points is sufficient to describe the spectra well and, in particular, to reproduce the highly anisotropic neutrino distribution outside the neutrinosphere.

Another, completely different approach to solve the Boltzmann equation is the Monte Carlo (MC) method by which the probabilistic history of a large number of sample neutrinos is followed to simulate the neutrino transport statistically (Tubbs 1978; Janka 1987, 1991a; Janka & Hillebrandt 1989a). In principle, the accuracy of the results is only limited by the statistical fluctuations associated with the finite number of sample particles. Since the MC transport essentially does not require the use of angle and energy grids, it allows one to cope with highly anisotropic angular distributions and to treat with high accuracy neutrino reactions with an arbitrary degree of energy exchange between neutrinos and matter. However, the MC method is also computationally very time consuming, in particular if high accuracy on a fine spatial grid or at high optical depths is needed. Therefore it is not the transport scheme of one's choice for coupling it with a hydrodynamics code.

In the present work, we make use of the advantages of the MC method in order to test the accuracy and reliability of a newly developed neutrino transport code that follows the lines of the S_N scheme described by Mezzacappa & Bruenn (1993a,b,c). In particular, we shall test the influence of the number of radial, energy, and angular mesh points on predicting the spectra and the radial evolution of the neutrino flux in “realistic” protoneutron star atmospheres as found in hydrodynamic simulations of supernova explosions (Wilson 1988). Since our investigations are restricted to static and time-independent backgrounds, we concentrate on generic properties of the transport description which should also hold for more general situations. The radial evolution of the angular distribution of the neutrinos is such a property, because it is primarily dependent on the profile of the opacity and the geometry of the neutrino-decoupling region, but is not very sensitive to the details of the temperature and composition in the neutron star atmosphere. Finally, good overall agreement of the MC and S_N results would strengthen the credibility of the MC transport with its limited ability to yield high spatial resolution.

The paper is organized as follows. The details of the Boltzmann solver and essential information for the MC method are given in Sect. 2. In Sect. 3 we describe the background models. Section 4 presents the results of our comparative calculations, i.e., neutrino spectra, luminosities, and Eddington factors. Some of our calculations are also compared against results obtained with a MGFLD code developed by Suzuki (1994). The dependence of the results from the S_N scheme on the energy, angular, and radial grid resolution is discussed, too. It is shown that an angular mesh that varies with the position in the star can

improve the angular resolution and the representation of the beamed neutrino distributions without increasing the number of angular mesh points. Finally, a summary of our results and a discussion of their implications can be found in Sect. 5.

2. Numerical methods

2.1. Boltzmann solver

2.1.1. Basic equations

Our S_N code is based on a finite difference form of the general relativistic Boltzmann equation for neutrinos. We assume spherical symmetry of the star throughout this paper. For the Misner-Sharp metric (Misner & Sharp 1964):

$$ds^2 = e^{2\phi(t,m)} c^2 dt^2 - e^{2\lambda(t,m)} \left(\frac{G}{c^2} \right)^2 dm^2 - r^2(t,m) (d\theta^2 + \sin^2 \theta d\phi^2) \quad , \quad (2)$$

the Boltzmann equation in the Lagrangian frame takes the following form:

$$\begin{aligned} & \frac{1}{c} e^{-\phi} \frac{\partial}{\partial t} \left(\frac{f_\nu}{\rho_b} \right) + 4\pi e^{-\phi} \mu \frac{\partial}{\partial m} \frac{e^{\phi} r^2 f_\nu}{m} \\ & + \frac{\partial}{\partial \mu} \left\{ (1 - \mu^2) \left[2\pi \rho_b \frac{\partial r^2}{\partial m} \right. \right. \\ & + \left. \left. \mu \frac{1}{c} e^{-\phi} \frac{\partial \ln(\rho_b r^3)}{\partial t} - 4\pi r^2 \rho_b \frac{\partial \phi}{\partial m} \right] \left(\frac{f_\nu}{\rho_b} \right) \right\} \\ & + \left[\mu^2 \frac{1}{c} e^{-\phi} \frac{\partial \ln(\rho_b r^3)}{\partial t} - \frac{1}{c} e^{-\phi} \frac{\partial \ln r}{\partial t} \right. \\ & - \left. \mu 4\pi r^2 \rho_b \frac{\partial \phi}{\partial m} \right] \frac{\partial}{\partial \frac{1}{3} \varepsilon_\nu^3} \left\{ \varepsilon_\nu^3 \left(\frac{f_\nu}{\rho_b} \right) \right\} \\ & = \frac{1}{\rho_b} \frac{1}{c} e^{-\phi} \left(\frac{\delta f_\nu}{\delta t} \right)_{\text{coll}} \quad . \end{aligned} \quad (3)$$

In the above formula c and G are the velocity of light and the gravitational constant, respectively, t is the coordinate time and m is the baryonic mass coordinate which is related to the circumference radius r through the conservation law of the baryonic mass. In view of combination with a Lagrangian hydrodynamics code (Yamada 1997), the baryonic mass is chosen to be the independent variable instead of the radius. ϕ , λ and r are the metric components which are determined by the Einstein equations. In this paper, however, these quantities are given from the background models and set to be constant with time during the neutrino transport calculations. f_ν is the neutrino phase space distribution function. Under the assumption of spherical symmetry, f_ν is a function of t , m , μ and ε_ν ,

where μ is the cosine of the angle of the neutrino momentum with respect to the outgoing radial direction and ε_ν is the neutrino energy. ρ_b is the baryonic mass density.

The right hand side of Eq. (3) is the so-called collision term, which actually includes absorption, emission, scattering and pair creation and annihilation of neutrinos, details of which are described below. The left hand side, on the other hand, looks a little bit different from the form used, for example, in Mezzacappa et al. (1993a,b,c). This is not only because it is fully general relativistic but also because all the velocity dependent terms are expressed as time derivatives so that it can easily be coupled to the implicit general relativistic Lagrangian hydrodynamics code (Yamada 1997). In this way a fully coupled, implicit system of the radiation-hydrodynamics equations is formed, in which the time derivatives can be treated easily because they are just off-diagonal components of the matrix set up from the linearized equations. It should be noted, however, that since we assume that the matter background is static in this paper, all these time derivatives are automatically set to be zero, although these terms have been already implemented in the code.

The conserved neutrino number N_ν in the absence of source terms is represented in terms of the chosen independent variables as

$$N_\nu = \int f_\nu(t, m, \mu, \varepsilon_\nu) \frac{dm}{\rho_b} \frac{2\pi \varepsilon_\nu^2 d\varepsilon_\nu d\mu}{(hc)^3} \quad . \quad (4)$$

This suggests to cast Eq. (3) in a conservation form with respect to the neutrino number. It is also evident that the combination of $\left(\frac{f_\nu}{\rho_b} \right)$ is more convenient to be used than f_ν itself. In the following, therefore, we define the specific neutrino distribution function as in Mezzacappa et al. (1993a,b,c) by

$$F_\nu \equiv \left(\frac{f_\nu}{\rho_b} \right) \quad (5)$$

and use this quantity as the dependent variable to be solved for.

2.1.2. Finite difference scheme of Boltzmann equations

As mentioned above the specific neutrino distribution function F_ν is a function of t , m , μ and ε_ν . This four-dimensional phase space is discretized and Eq. (3) is written as a finite-difference equation. In the time direction we adopt a fully implicit differencing. The discretized specific distribution function $F_{i,j,k}^n$ is defined at the mesh centers of the spatial, angular and energy grids. Here the subscripts i, j, k refer to the spatial, angular and energy grid points, respectively. The superscript n corresponds to the time step. The value at each cell interface is evaluated by interpolation of the distribution at two adjacent mesh centers.

Our finite difference method is essentially the same as that of Mezzacappa et al. (1993a,b,c) with some modifications. For the spatial advection, the upwind difference and the centered difference are linearly averaged with the weights determined by the ratio of the mean free path to the distance to the stellar surface unlike Mezzacappa et al. (1993a,b,c) who used the ratio of the mean free path to the local mesh width. In fact, in the latter case we found that the upwind distribution was given too large a weight in the optically thick region and thus the flux was overestimated. This issue will be addressed later.

The angular mesh is determined such that each mesh center and cell width correspond to the abscissas and weights of the Gauss-Legendre quadrature, respectively. In angular direction, the neutrino distribution at each interface is simply taken as the upwind value. The advection in the energy space is also approximated by an upwind scheme following Mezzacappa & Matzner (1989), although this does not allow to conserve both lepton number and energy in non-static situations (which are not considered here) unless a large number of energy zones is used (Mezzacappa, private communication).

In typical calculations, 105, 6 and 12 mesh points are used for the spatial, angular and energy discretizations, respectively. The dependence of the results on the numbers of mesh points will be discussed below. The finite-differenced Boltzmann equation forms a nonlinear coupled system of equations for all radial grid points which is linearized and solved iteratively by using a Newton-Raphson scheme. The linearized equations adopt a block tridiagonal matrix form, which can be efficiently solved by the Feautrier method.

2.2. Monte Carlo method

Different from the finite difference method, the Monte Carlo method constructs the statistical ensemble average by following the destinies of individual test particles and performing the average when all particles have been transported. Due to the fact that neutrinos are fermions it is impossible to propagate them independently. Instead, the full time-dependent problem has to be simulated by following a large number (typically $\sim 500,000$) of sample particles along their trajectories simultaneously in order to be able to construct the local phase space occupation functions and to include anisotropies as well as phase space blocking effects self-consistently into the calculation of the reaction rates and source terms. The modeling of the phase space distribution function from the local particle sample must guarantee the correct approach to chemical equilibrium. Also the Pauli exclusion principle has to be satisfied by the statistical average. We refer readers to Janka (1987) and references therein for details.

The stellar background is divided into 15 equispaced spherical shells of homogeneous composition and uniform thermodynamical conditions, the number of which was

determined both from physical requirements for spatial resolution and from the requirement to have acceptably small statistical errors in the local neutrino phase space distributions constructed from the chosen number of sample particles. Although the Monte Carlo method is essentially mesh free, about 60 energy bins and approximately 35 angular bins are used only for representing the phase space distribution functions and for calculating the reaction kernels. Neutrinos are injected into the computational volume at the inner boundary in the way described in the next section, while particles passing inwardly through the inner boundary are simply forgotten. The outer boundary is treated as a free boundary, where particles escape unhindered and no neutrino is assumed to come in from outside.

2.3. Boundary conditions

In the presented calculations we are mainly interested in the neutrino transport in the region where the neutrinos decouple from the stellar background and the emitted spectra form. Therefore we calculate the neutrino transport only in the vicinity of the “neutrinosphere”. For this reason we have to set an inner boundary condition as well as an outer boundary condition for each model. At the outer boundary we impose the condition that no neutrinos enter the computational volume from outside. In the Boltzmann solver, this is realized by setting

$$f_\nu(r_s, \mu, \varepsilon_\nu) = \begin{cases} f_\nu(r_{\max}, \mu, \varepsilon_\nu) & \text{for } \mu \geq 0 \\ 0 & \text{for } \mu < 0, \end{cases} \quad (6)$$

where r_{\max} is the radius of the outermost mesh center, and r_s is the radius of the outer surface which is dislocated outward from the outermost mesh center by half a radial cell width.

On the other hand, we have to specify the distribution of the neutrinos coming into the computational volume at the inner boundary r_{IB} which is dislocated inward from the innermost mesh center r_{\min} by half a radial cell width. For this purpose we adopt Fermi-Dirac distribution functions, in which the temperature, chemical potential and a normalization factor are determined such that the neutrino number density at r_{IB} (where the neutrinos are essentially isotropically distributed because the inner boundary is chosen to be located at high optical depth), the average energy $\langle \varepsilon_\nu \rangle$ and the width of the energy spectrum, measured by the parameter $\frac{\langle \varepsilon_\nu^2 \rangle}{\langle \varepsilon_\nu \rangle^2}$ (see Janka & Hillebrandt 1989b), are reproduced as given by Wilson’s (1988) models. Thus the inner boundary condition is set as :

$$f_\nu(r_{\text{IB}}, \mu, \varepsilon_\nu) = \begin{cases} \frac{1}{A} \frac{1}{e^{(\varepsilon_\nu - \mu_{\text{IB}})/(k_B T_{\text{IB}})} + 1} & \text{for } \mu \geq 0 \\ f_\nu(r_{\min}, \mu, \varepsilon_\nu) & \text{for } \mu < 0 \end{cases}, \quad (7)$$

where A , μ_{IB} and T_{IB} are the fitting parameters, the values of which are summarized in Table 1 for all considered models and neutrino species. Concerning the distribution of neutrinos that leave the computational volume, we impose in Eq. (7) in the Boltzmann solver the condition that it is the same as the distribution at the innermost mesh center. From the physical point of view, however, and treated correctly in the Monte Carlo simulations, it should be determined by the fraction of neutrinos which is emitted or backscattered towards the inner boundary. This is in general different from what the phase space distribution at the innermost mesh center yields because the mean free path of the neutrinos near the inner boundary is shorter than the mesh width. As a result the imposed condition for $\mu < 0$ in Eq. (7) leads to a minor discrepancy of the treatment of the inner boundary condition in the Monte Carlo and Boltzmann computations and sometimes causes a small oscillation of the neutrino distribution near the inner boundary in the latter computations. This issue will be revisited later.

Table 1. Fitting parameters for the Fermi-Dirac distributions which describe the spectra at the inner boundary.

models	neutrinos	T_{IB} [MeV]	μ_{IB} [MeV]	A
W1	ν_e	9.56932	7.85190	1.221490
	$\bar{\nu}_e$	9.38259	7.13610	3.874140
	ν_μ	10.32539	30.87195	17.911456
W2	$\bar{\nu}_e$	10.52454	5.75932	3.672680
W3	$\bar{\nu}_e$	9.87875	11.27370	7.108076

2.4. Input physics

2.4.1. Neutrino reactions

The neutrino opacities of dense neutron star matter are still one of the major uncertainties of supernova simulations. Theoretical and numerical complications arise from the description and treatment of nucleon thermal motion and recoil (Schinder 1990), nuclear force effects and nucleon blocking (Prakash et al. 1997; Reddy et al. 1997), and nucleon correlations, spatial (Sawyer 1989; Burrows & Sawyer 1998a,b; Reddy et al. 1998a) as well as temporal (Raffelt & Seckel 1995; Raffelt et al. 1996). Although in particular nucleon recoil and auto-correlations might play an important role even in the sub-nuclear outer layers of the protoneutron star down to densities below $10^{13} \text{ g cm}^{-3}$ (Janka et al. 1996; Hannestad & Raffelt 1997) we do not concentrate on this problem here but rather employ the standard description of the neutrino opacities, according to which neutrinos interact with isolated nucleons (see, e.g., Tubbs & Schramm 1975; Bruenn 1985). Also,

as in most other simulations, bremsstrahlung production of neutrino-antineutrino pairs is neglected here, although it may be important as pointed out by Suzuki (1993) and more recently by Burrows (1997) and Hannestad & Raffelt (1997). Doing so, we intend to enable comparison with other (already published) work and want to avoid the mixing of effects from a different numerical treatment of the transport with those from a non-standard description of neutrino-nucleon interactions or from the inclusion of processes typically not considered in the past.

The following neutrino reactions have been implemented in our codes.

- [1] $\nu_e + n \rightleftharpoons e + p$
(electron-type neutrino absorption on neutrons),
- [2] $\bar{\nu}_e + p \rightleftharpoons e^+ + n$
(electron-type anti-neutrino absorption on protons),
- [3] $\nu + N \rightleftharpoons \nu + N$
(neutrino scattering on nucleons),
- [4] $\nu + e \rightleftharpoons \nu + e$
(neutrino scattering on electrons).

In addition to the above reactions, the following processes have also been implemented in both codes, although these reactions are not used in the present paper.

- [5] $\nu_e + A \rightleftharpoons A + e^-$
(electron-type neutrino absorption on nuclei),
- [6] $\nu + A \rightleftharpoons \nu + A$
(neutrino coherent scattering on nuclei),
- [7] $e^- + e^+ \rightleftharpoons \nu + \bar{\nu}$
(electron-positron pair annihilation and creation),
- [8] $\gamma^* \rightleftharpoons \nu + \bar{\nu}$
(plasmon decay and creation).

Since the pair processes are not taken into account in this paper, we can treat each species of neutrinos separately. A test showed that in the considered protoneutron star atmospheres neutrino pair creation and annihilation as well as processes involving nuclei are unimportant to determine the fluxes and spectra.

2.4.2. EOS

In this paper we use a simplified equation of state, in which only nucleons, electrons, alpha particles and photons are included. They are all treated as ideal gases. For given density, temperature and electron fraction we derive the mass fractions and the chemical potentials of nucleons and the electron chemical potential from this equation of state. The disregard of nuclei is well justified for the densities and temperatures we are considering, where most of the nuclei are dissociated into free nucleons. This is actually confirmed by comparing our EOS with the more realistic EOS of Wolff that is based on the Skyrme-Hartree-Fock method (Hillebrandt & Wolff 1985). Only very small

differences of the nucleon chemical potentials are found for the innermost region where small amounts of nuclei appear and for the outermost region where some contribution from alpha particles is mixed into the stellar medium. We also repeated some of the calculations making use of the Wolff EOS with the nuclei-related reactions [5], [6] (neutrino emission, absorption and scattering on nuclei) turned on and found qualitatively and quantitatively the same results. Hence the nuclei-related reactions are switched off in the calculations described below.

3. Models

3.1. Stellar models

The time-dependent transport calculations presented here were performed for background profiles which are representative of protoneutron star atmospheres during the quasi-static neutrino cooling phase (Wilson 1988). At this stage, several seconds after core bounce, the typical evolution timescale of density, temperature, and electron fraction is much longer than the timescale for neutrinos to reach a stationary state. Therefore our assumption of a static and time-independent background is justified. In addition, our interest is focused on the radial evolution of the Eddington factors and on a test of the influence of the energy and angle resolution used in the S_N Boltzmann solver. Both aims do not require a fully self-consistent approach which takes into account the evolution of the stellar background (in particular of the temperature and composition). In fact, the Eddington factors are normalized angular integrals of the radiation intensity and as such reflect very general characteristics of the geometrical structure of the atmosphere where neutrinos and matter decouple.

Profiles from Wilson's (1988) protoneutron star model were taken for three different times, 3.32, 5.77, and 7.81 s after core bounce. With the chosen fundamental variables density ρ , temperature T , and electron fraction Y_e , the thermodynamical state is defined for the plasma consisting of non-relativistic free nucleons, arbitrarily relativistic and degenerate electrons and positrons, and photons in thermal equilibrium. Figures 1–3 show the input used for the three models. In Fig. 3 also the general relativistic metric coefficients $\sqrt{g_{tt}} = e^\phi$ and $\sqrt{-g_{rr}} = e^\lambda$ are given as provided by Wilson's data and used for a comparative general relativistic calculation of the neutrino transport in model W3.

3.2. Computed transport models

All models computed with the Boltzmann code are summarized in Table 2. Models ST are the standard models, in which 105 uniform spatial, 6 angular and 12 energy mesh points were used. The energy mesh is logarithmically uniform and covers 0.9 – 110 MeV. The numbers of angular grid points and energy grid points were increased in models FA and FE, respectively. In model CS we used the

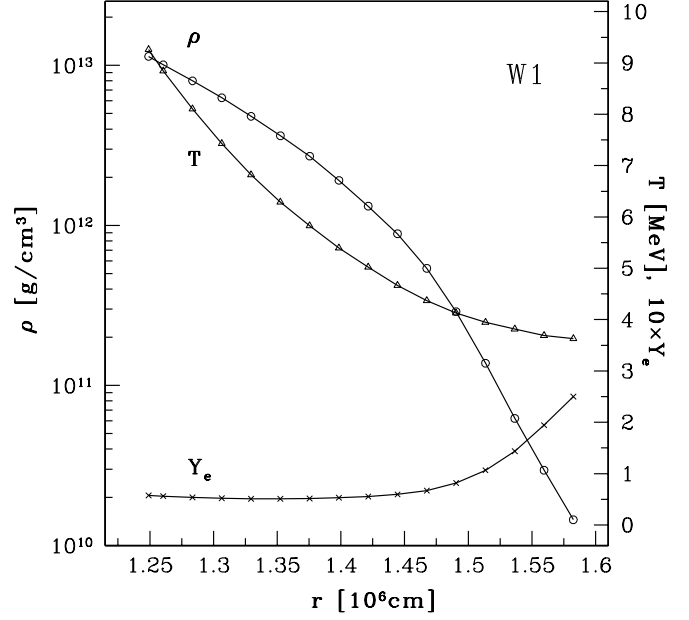


Fig. 1. The profile of density, temperature and electron fraction for Wilson's (1988) post bounce core model W1 ($t = 3.32$ s).

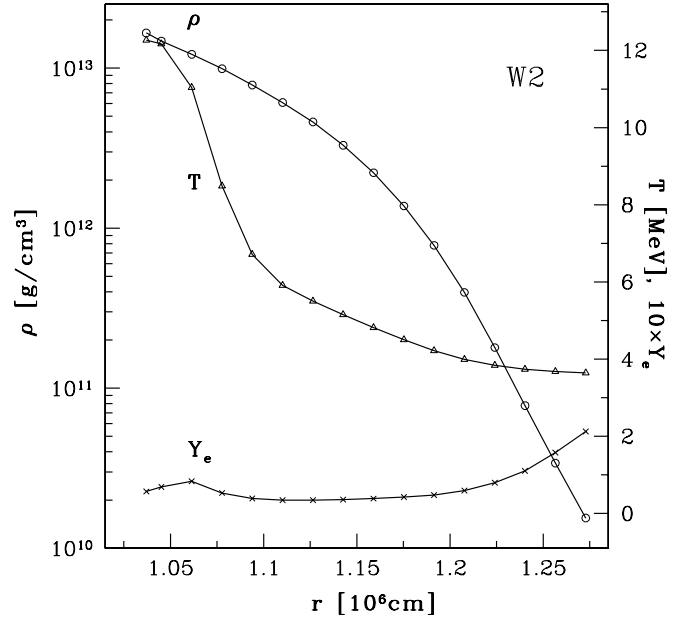


Fig. 2. The profile of density, temperature and electron fraction for Wilson's post bounce core model W2 ($t = 5.77$ s).

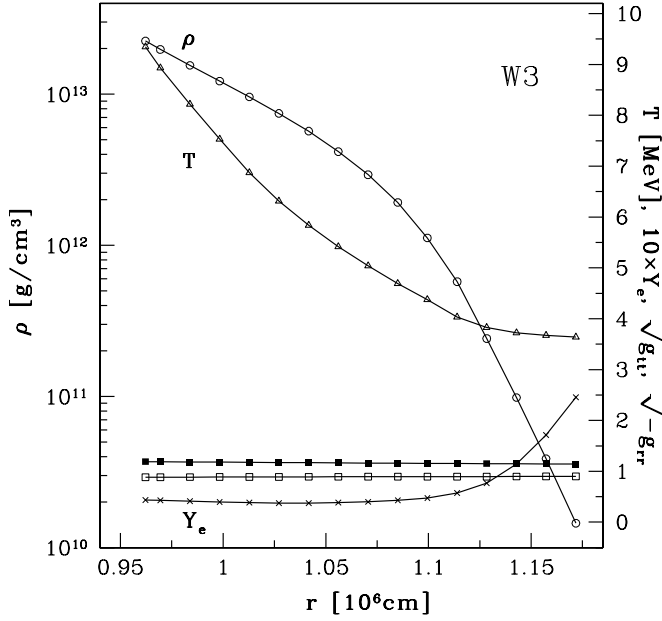


Fig. 3. The profile of density, temperature and electron fraction as well as the metric coefficients $\sqrt{g_{tt}}$ (open squares) and $\sqrt{-g_{rr}}$ (filled squares) for Wilson's post bounce core model W3 ($t = 7.81$ s).

same radial grid as in the Monte Carlo simulations where 15 radial zones were chosen. 105 spatial mesh points were again used in model NI with no interpolations of density, temperature and electron fraction in the radial grid of the Monte Carlo simulations. Model GR took into account the general relativistic effects. We used a non-uniform spatial mesh in model NU. A different interpolation of up-wind differencing and centered differencing was tried for the radial advection term in model DI. We assumed the nucleon scattering to be isotropic in model IS. As is understood from Table 2, most of the comparisons were done for the electron-type anti-neutrinos, since they are most important from the observational point of view.

4. Numerical results

4.1. Luminosity and average energy

In the following, we consider the neutrino transport results after the time-dependent simulations have reached steady states.

First we compare observable quantities such as the luminosity, average energy and average squared energy of the neutrino flux for models ST and GR. These quantities

are calculated at the outermost spatial zone as

$$L_\nu = 4\pi r_s^2 c \int \frac{2\pi \varepsilon_\nu^2 d\varepsilon_\nu d\mu}{(hc)^3} f_\nu \mu \varepsilon_\nu \quad , \quad (8)$$

$$\langle \varepsilon_\nu \rangle = \frac{\int \frac{2\pi \varepsilon_\nu^2 d\varepsilon_\nu d\mu}{(hc)^3} f_\nu \mu \varepsilon_\nu}{\int \frac{2\pi \varepsilon_\nu^2 d\varepsilon_\nu d\mu}{(hc)^3} f_\nu \mu} \quad , \quad (9)$$

$$\langle \varepsilon_\nu^2 \rangle = \frac{\int \frac{2\pi \varepsilon_\nu^2 d\varepsilon_\nu d\mu}{(hc)^3} f_\nu \mu \varepsilon_\nu^2}{\int \frac{2\pi \varepsilon_\nu^2 d\varepsilon_\nu d\mu}{(hc)^3} f_\nu \mu} \quad , \quad (10)$$

where r_s is again the surface radius, and the redshift corrections from the surface up to infinity are not taken into account. The results are summarized in Table 3.

The electron-type neutrino has the lowest energy while the muon-type neutrino has the highest. The reason for this is that the electron-type neutrino has the shortest mean free path due to absorptions on the abundant neutrons, and decouples in the surface-near layers where the temperature is lower. In contrast, the muon and tau neutrinos do not interact with particles of the stellar medium by charged currents and therefore their thermal decoupling occurs at a higher temperature. The luminosity for the electron-type anti-neutrino gets smaller as time passes, which is due to the cooling and shrinking of the protoneutron star. As can be seen in the table, the agreement of all quantities between the two methods is very good, which confirms the statistical convergence of the Monte Carlo simulations. The average energy is in general determined accurately because the energy spectrum is shaped in the region where the neutrino angular distribution is not very anisotropic. Moreover, possible effects due to the rather coarse angular resolution of the Boltzmann code essentially cancel out by taking the ratios of Eqs. (9) and (10). On the other hand, the luminosity and the number flux of the Monte Carlo computations are also well reproduced by the Boltzmann results. This is due to the fact that these quantities are also determined deep inside the star and are nearly conserved farther out. In fact, when integrating Eq. (3) over angle and energy multiplying with unity and ε_ν , respectively, ignoring all time derivatives and general relativistic effects, one gets

$$\frac{\partial F_\nu^n(r)}{\partial m} = \frac{1}{\rho_b} \int \frac{2\pi \varepsilon_\nu^2 d\varepsilon_\nu d\mu}{(hc)^3} \left(\frac{\delta f_\nu}{\delta t} \right)_{\text{coll}} \quad , \quad (11)$$

$$\frac{\partial L_\nu^\varepsilon(r)}{\partial m} = \frac{1}{\rho_b} \int \frac{2\pi \varepsilon_\nu^2 d\varepsilon_\nu d\mu}{(hc)^3} \varepsilon_\nu \left(\frac{\delta f_\nu}{\delta t} \right)_{\text{coll}} \quad , \quad (12)$$

where $F_\nu^n(r)$ and $L_\nu^\varepsilon(r)$ are the number and energy fluxes of neutrinos at radius r , respectively, and defined as,

$$F_\nu^n(r) = 4\pi r^2 c \int \frac{2\pi \varepsilon_\nu^2 d\varepsilon_\nu d\mu}{(hc)^3} f_\nu \mu \quad , \quad (13)$$

$$L_\nu^\varepsilon(r) = 4\pi r^2 c \int \frac{2\pi \varepsilon_\nu^2 d\varepsilon_\nu d\mu}{(hc)^3} f_\nu \mu \varepsilon_\nu \quad . \quad (14)$$

Table 2. Characteristics of the calculated models. $105_r \times 6_\mu \times 12_\varepsilon$ implies that 105 spatial mesh points, 6 angular mesh points and 12 energy mesh points are used. See the text for details.

model	mesh	background model	ν species	notes
ST1	$105_r \times 6_\mu \times 12_\varepsilon$	W1	ν_e	interpolation in spatial grid of MC
ST2	$105_r \times 6_\mu \times 12_\varepsilon$	W1	$\bar{\nu}_e$	interpolation in spatial grid of MC
ST3	$105_r \times 6_\mu \times 12_\varepsilon$	W2	$\bar{\nu}_e$	interpolation in spatial grid of MC
ST4	$105_r \times 6_\mu \times 12_\varepsilon$	W3	$\bar{\nu}_e$	interpolation in spatial grid of MC
ST5	$105_r \times 6_\mu \times 12_\varepsilon$	W1	ν_μ	interpolation in spatial grid of MC
FA	$105_r \times 10_\mu \times 12_\varepsilon$	W1	$\bar{\nu}_e$	interpolation in spatial grid of MC
FE	$105_r \times 6_\mu \times 18_\varepsilon$	W1	$\bar{\nu}_e$	interpolation in spatial grid of MC
CS	$15_r \times 6_\mu \times 12_\varepsilon$	W1	$\bar{\nu}_e$	same spatial grid as in MC
NI	$105_r \times 6_\mu \times 12_\varepsilon$	W1	$\bar{\nu}_e$	no interpolation in spatial grid of MC
GR	$105_r \times 6_\mu \times 12_\varepsilon$	W3	$\bar{\nu}_e$	general relativity included
NU	$105_r \times 6_\mu \times 12_\varepsilon$	W1	$\bar{\nu}_e$	non-uniform spatial mesh
DI	$105_r \times 6_\mu \times 12_\varepsilon$	W1	ν_μ	different interpolation for conservative radial advection
IS	$105_r \times 6_\mu \times 12_\varepsilon$	W1	$\bar{\nu}_e$	isotropic ν - N scattering

Table 3. Luminosity, average energy and average squared energy for models ST1–ST5 and for model GR. B and MC in the second column refer to the Boltzmann simulations and the Monte Carlo simulations, respectively. For the definitions of L_ν , $\langle \varepsilon_\nu \rangle$ and $\langle \varepsilon_\nu^2 \rangle$ see Eqs. (8), (9) and (10) in the text.

		ν_e W1	$\bar{\nu}_e$ W1	$\bar{\nu}_e$ W2	$\bar{\nu}_e$ W3	ν_μ W1	$\bar{\nu}_e$ GR, W3
L_ν	B	7.1×10^{51}	4.0×10^{51}	2.5×10^{51}	1.5×10^{51}	4.9×10^{51}	1.3×10^{51}
[erg/sec]	MC	7.3×10^{51}	4.0×10^{51}	2.6×10^{51}	1.5×10^{51}	4.9×10^{51}	1.3×10^{51}
$\langle \varepsilon_\nu \rangle$	B	12.8	16.3	15.9	16.2	24.3	15.5
[MeV]	MC	12.7	16.1	15.8	16.3	24.2	15.6
$\langle \varepsilon_\nu^2 \rangle$	B	198.5	329.0	309.9	324.5	727.8	300.3
[MeV ²]	MC	198.6	322.6	308.9	327.1	724.3	300.6

As expected intuitively, the scattering kernels drop out of the right hand side of Eq. (11) while only the isoenergetic scattering does not contribute on the right hand side of Eq. (12). In the given Boltzmann code Eqs. (11) and (12) are discretized in a conservative form for the radial advection. Therefore it is clear that the Boltzmann code can calculate the number and energy fluxes accurately if also the number and energy exchange by the reactions are calculated accurately in the source terms on the right hand sides of the equations. Moreover, the radial evolutions of $F_\nu^n(r)$ and $L_\nu^\varepsilon(r)$ are entirely determined by the number and energy exchange through reactions of which the net effect is small in an atmospheric layer which is in a stationary state and reemits as much energy and lepton number as it absorbs. Changes of the number fluxes and luminosities in the considered protoneutron star atmospheres occur only in regions where the neutrino distribution is still essentially isotropic and possible effects due to an insufficient angular resolution in the Boltzmann S_N scheme do not cause problems. For all these reasons it is not surprising that the same quality of agreement is also found

for the radial evolutions of the luminosity, average energy and average squared energy and that this is also true for the general relativistic case.

4.2. Neutrino energy spectra

In the previous section we discussed only the energy and angle integrated quantities. However, we also provide information about the energy spectra of each neutrino species, because they yield more evidence about the quality of the agreement between the calculations with the different codes.

Figs. 4 and 5 show energy flux spectra defined as

$$\frac{1}{4\pi r_s^2 c} \frac{dL_\nu}{d\varepsilon_\nu} = \int \frac{2\pi d\mu}{(hc)^3} f_\nu \mu \varepsilon_\nu^3, \quad (15)$$

at the protoneutron star surface for different cases. For the reasons discussed in section 4.1, the spectra computed with the Boltzmann code (symbols) and the Monte Carlo code (lines) show excellent agreement. The number and the distribution of the energy bins in the Boltzmann code

seem to be adequate to reproduce the highly resolved Monte Carlo spectra.

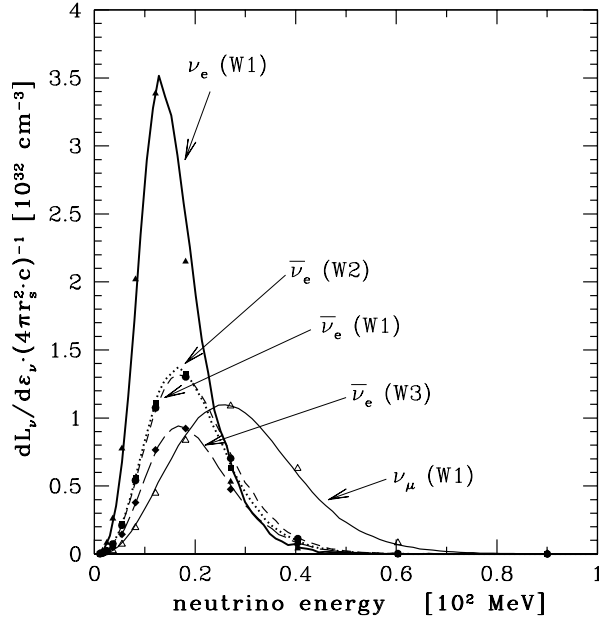


Fig. 4. The neutrino energy flux spectra at the protoneutron star surface. The lines show the results of the Monte Carlo simulations (the thick solid line, the short dashed line and the thin solid line for electron-type neutrinos, electron-type anti-neutrinos and muon-type neutrinos, respectively, in case of background model W1, and the dotted line and the long dashed line for electron-type anti-neutrinos in case of background models W2 and W3, respectively). The symbols represent the results of the corresponding Boltzmann simulations (the filled triangles, the filled circles and the open triangles for electron-type neutrinos, electron-type anti-neutrinos and muon-type neutrinos, respectively, in case of background model W1, and the filled squares and the filled diamonds for electron-type anti-neutrinos in case of background models W2 and W3, respectively).

4.3. Flux factor and Eddington factor

So far we discussed only angle integrated quantities since they are observable. However we are also interested in the angular distributions of the neutrinos, because information about the angular distributions is important to determine the neutrino heating rate in the hot-bubble region (see Eq. (1)). Although it is an advantage of the Boltzmann solver over MGFLD that one does not have to assume an ad hoc closure relation between the angular moments of the distribution function, one should remember that the usable number of angular mesh points is severely

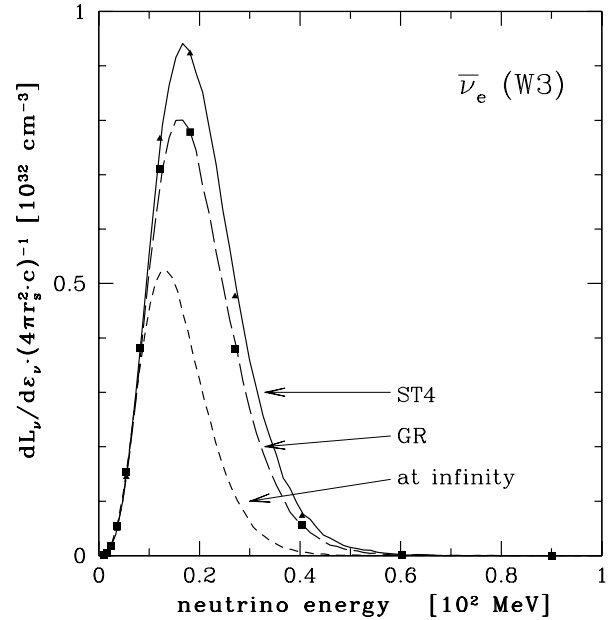


Fig. 5. The electron-type anti-neutrino energy flux spectra for background model W3 with and without general relativity. The long dashed line and the filled squares show the results of the Monte Carlo simulation and the Boltzmann simulation, respectively, with the general relativistic effects included. The solid line and the filled triangles are for the corresponding non-relativistic results. The short dashed line is the redshift-corrected energy spectrum at infinity calculated from the Monte Carlo results, the other results are given at the protoneutron star surface.

limited. In the Feautrier method the computation time increases in proportion to the third power of the dimension of the blocks in the tridiagonal block matrix which has to be inverted when one chooses the radius as the outermost variable of the do-loops. The dimension of one block, in turn, is linearly proportional to the number of angular mesh points. The same dependence holds for the number of energy mesh points and the number of neutrino species. In the standard calculations we use 6 angular mesh points and 12 energy grid points, and we treat a single neutrino species at a time, which corresponds to a block matrix size of 72. On the other hand, the number of spatial grid points is about 100. The CPU time is a few seconds per inversion of the whole matrix on a single vector processor of a Fujitsu VPP500. Hence, use of more than 10 angular mesh points is almost prohibitive for calculations with three neutrino species even with a highly parallelized matrix inversion routine (Sumiyoshi & Ebisuzaki 1998). It is, therefore, important to clarify the sensitivity of the accuracy to the angular resolution.

For this reason we consider the flux factor $\langle \mu \rangle_{e1}$ and the Eddington factor $\langle \mu^2 \rangle_{e1}$ which are defined as :

$$\langle \mu \rangle_{e1} = \frac{\int \frac{2\pi \varepsilon_\nu^2 d\varepsilon_\nu d\mu}{(hc)^3} f_\nu \mu \varepsilon_\nu}{\int \frac{2\pi \varepsilon_\nu^2 d\varepsilon_\nu d\mu}{(hc)^3} f_\nu \varepsilon_\nu}, \quad (16)$$

$$\langle \mu^2 \rangle_{e1} = \frac{\int \frac{2\pi \varepsilon_\nu^2 d\varepsilon_\nu d\mu}{(hc)^3} f_\nu \mu^2 \varepsilon_\nu}{\int \frac{2\pi \varepsilon_\nu^2 d\varepsilon_\nu d\mu}{(hc)^3} f_\nu \varepsilon_\nu}. \quad (17)$$

Here the subscript “e1” means that the averages are defined with the weight of energy. In MGFLD these factors are related with each other by a closure condition which can be derived from the employed flux-limiter (Janka 1991a, 1992). For simplicity we discuss here only energy integrated quantities as defined above. The fundamental features are similar for the individual energy groups.

In Figs. 6–8, we show the radial evolutions of the flux factors and the Eddington factors for all neutrino species in case of background model W1. The upper panels show the flux factors and the lower panels the corresponding Eddington factors. The solid lines are the results of the Boltzmann simulations (having the finer radial resolution) and the filled triangles are those of the Monte Carlo simulations. As can be seen, near the inner boundary the flux factors are almost zero while the Eddington factors are 1/3, which implies that the neutrino angular distribution is nearly isotropic, a consequence of the fact that the neutrinos are in equilibrium with the surrounding matter. As we move outward, both factors begin to deviate from these values, reflecting the increase of the mean free path and a more rapid diffusion. Farther out, the angular moments increase monotonically towards unity, the value in the free streaming limit, as the angular distribution gets more and more forward peaked with increasing distance from the source. As can be seen clearly in Figs. 6–8, the Boltzmann solver tends to *underestimate* both angular moments in the outermost region, where the neutrino angular distribution is most forward peaked. This can be explained by the insufficient angular resolution, or, to be more specific, by the fact that in case of the employed Gauss-Legendre quadrature the maximum angle cosine μ_{\max} of the angular grid is significantly less than unity, if not a large number of angular grid points is used. This is directly confirmed by using a larger number of angular mesh points or, in particular, a variable angular mesh (see Sect. 4.4).

The same trend is also present in the general relativistic case, model GR, as shown in Fig. 9. It turned out that the ray bending effect which tends to isotropize the angular distribution of the neutrinos is not very important and that differences between the Monte Carlo results and the Boltzmann results are significantly larger.

In Fig. 10 we show the flux factor and the Eddington factor for model FA where we employed 10 angular mesh points instead of 6. The long dashed lines are for model FA and the short dashed lines depict the result of model ST2, the corresponding standard model, for comparison. The discrepancy between the Boltzmann simulation and the Monte Carlo simulation is reduced with the increase of the number of angular mesh points. This supports our interpretation that the deviation stems entirely from the insufficient angular resolution and/or the unfavorable location of the angular grid points for the Gauss-Legendre quadrature used in the Boltzmann simulations. Indeed, the degree of improvement is consistent with the fact that our finite difference scheme is of first order for the angular advection, since we always take the upwind differencing as explained above. Even with the finer 10-zone angular mesh the deviation of both factors from the exact values given by the Monte Carlo result is significant. The maximum deviations, $1 - \mu_{\max}$ for the flux factor and $1 - \mu_{\max}^2$ for the Eddington factor, are approached as one goes farther out into the optically thin regime. This is visible in Fig. 11 which displays the ratios of the Boltzmann to the Monte Carlo results for the flux factors and the Eddington factors in case of 6 and 10 angular bins and the variable angular mesh. (The relatively large discrepancies of the flux factors for smaller radii are explained by slight differences of the treatment of the inner boundary condition, see Sect. 2.3, and by the fact that the flux factor adopts very small values in the optically thick region.) It should be mentioned that the flux factors calculated in the recent paper by Messer et al. (1998) do not converge to unity but saturate at a nearly constant lower level (around 0.9) even far outside of the neutrinosphere. This reflects the use of $\mu_{\max} = 0.93$ for the largest μ -bin of the angular grid in the 6-point quadrature of the S_6 method.

It is interesting to see that this tendency of the Boltzmann solver is completely opposite to that of MGFLD. Janka (1991a, 1992) pointed out that all flux limiters used so far tend to overestimate the flux factor and the Eddington factor in the optically thin region, which implies that the neutrino angular distribution approaches the free streaming limit much too rapidly (see also Messer et al. 1998). In order to confirm this statement, transport calculations with MGFLD were done for the same models with three different flux limiters, which are Bruenn’s (BR), Levermore & Pomraning’s (LP) and Mayle & Wilson’s (MW). We refer readers to Janka (1992) and Suzuki (1994) and references therein for details on the flux limiters. We show in Figs. 12 and 13 the flux factors and local number densities of the electron-type neutrino and electron-type anti-neutrino for model W1, respectively. It is clear that all flux limiters overestimate the forward peaking of the angular distributions of the neutrinos in the optically thin region, a trend that holds for all neutrino species and is not dependent on the background model. The typical deviation of MGFLD results from the

Monte Carlo results is much larger than that between the Boltzmann solver and the Monte Carlo method.

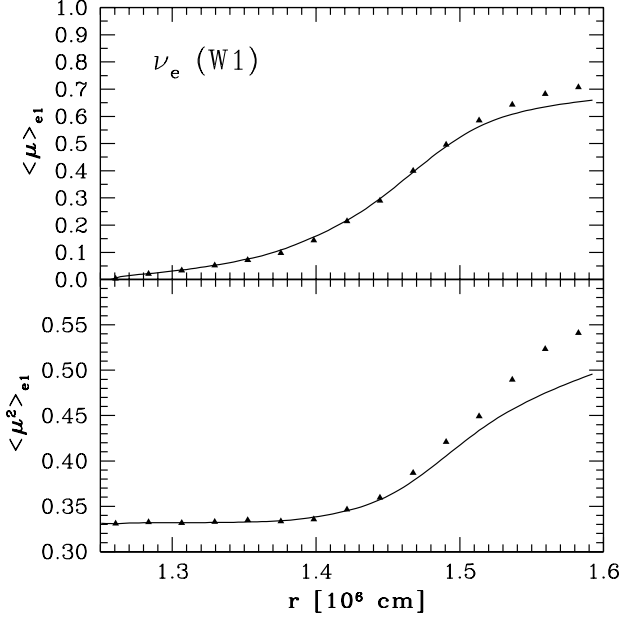


Fig. 6. The flux factor (upper panel) and the Eddington factor (lower panel) of the electron-type neutrino for model W1. The filled triangles and the solid line show the results of the Monte Carlo simulation and the Boltzmann simulation, respectively.

From the lower panels of Figs. 12 and 13 we learn that the local neutrino number density, which is given by

$$n_\nu(r) = \int \frac{2\pi\varepsilon_\nu^2 d\varepsilon_\nu d\mu}{(hc)^3} f_\nu \quad , \quad (18)$$

is overestimated in case of the Boltzmann solver (by about 10%) and underestimated for MGFLD (by approximately 30%) in the optically thin region. This is understood from the fact that the number flux, which is defined as

$$F_\nu^n(r) = 4\pi r^2 c \int \frac{2\pi\varepsilon_\nu^2 d\varepsilon_\nu d\mu}{(hc)^3} f_\nu \mu \quad , \quad (19)$$

is related to the local neutrino number density by

$$n_\nu(r) = \frac{F_\nu^n(r)}{4\pi r^2 c \langle\mu\rangle_{e0}} \quad . \quad (20)$$

$\langle\mu\rangle_{e0}$ denotes the average angle cosine for the neutrino number flux and is calculated from Eq. (16) with a factor ε_ν omitted under the integrals in the numerator and denominator. Since the number flux is determined deep inside the protoneutron star atmosphere where the neutrinos are still nearly isotropic, and conserved farther out,

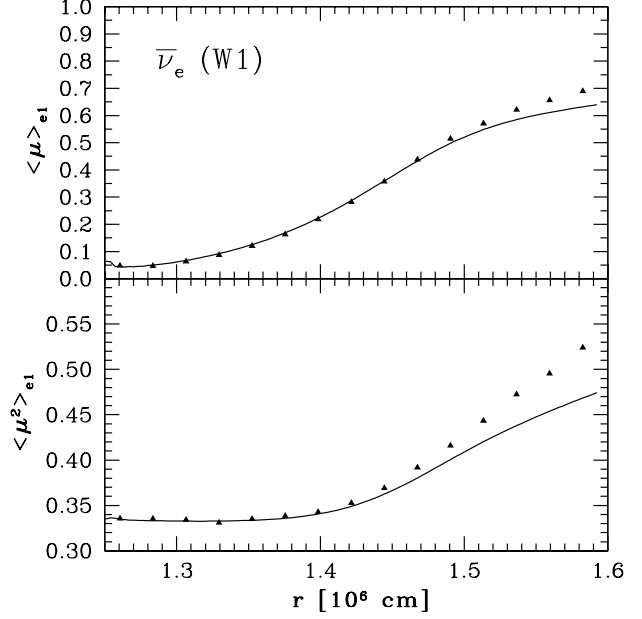


Fig. 7. The same as Fig. 6 but for the electron-type anti-neutrino.

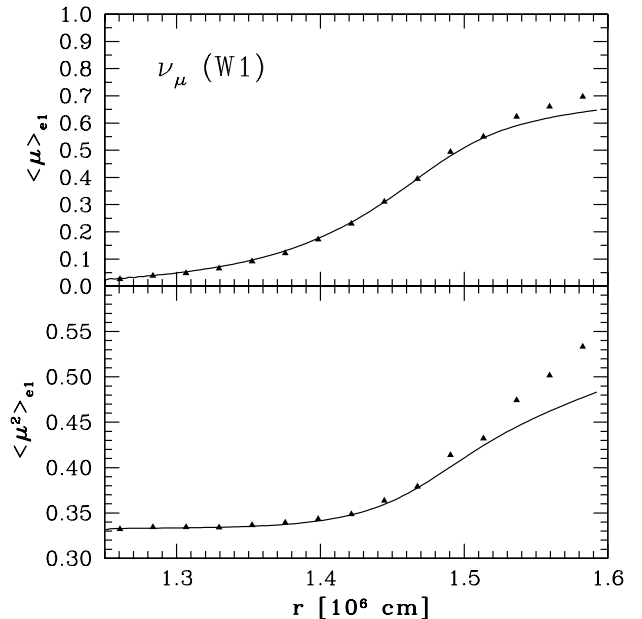


Fig. 8. The same as Fig. 6 but for the muon-type neutrino.

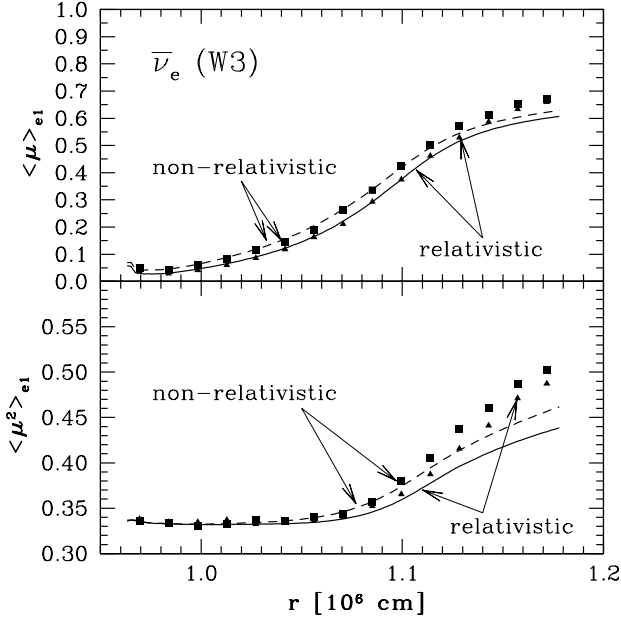


Fig. 9. The flux factor (upper panel) and the Eddington factor (lower panel) of the electron-type anti-neutrino for model GR where the general relativistic effects are taken into account. The solid line represents the results of the Boltzmann simulation while the solid triangles correspond to those of the Monte Carlo simulation. For comparison the corresponding non-relativistic results, model ST4, are shown with the solid squares and the dashed lines for the Monte Carlo simulation and the Boltzmann simulation, respectively.

it is not affected by problems with a coarse angular resolution occurring in the optically thin regime. For this reason, the number and energy fluxes agree well between the Monte Carlo method and the Boltzmann solver irrespective of the angular resolution as long as the Boltzmann solver is based on conservative finite differencing in the radial direction. The good agreement of the fluxes is confirmed by Fig. 14, which depicts the radial behavior of the number flux in case of models ST1, ST2 and ST5.

It is now clear from Eq. (20) that an underestimation (overestimation) of the flux factor leads to an overestimation (underestimation) of the number density, if the flux is the same. It should be noted that even in the outermost zone of our computational region in the atmosphere of a protoneutron star, the neutrino angular distribution is not so strongly forward peaked as in the hot-bubble region farther out. Hence it must be expected that the errors by an over- or underestimation of the neutrino number density might be even larger in the hot-bubble region where neutrino heating takes place.

Since the neutrino heating rate is proportional to the local neutrino number density (actually: energy density)—

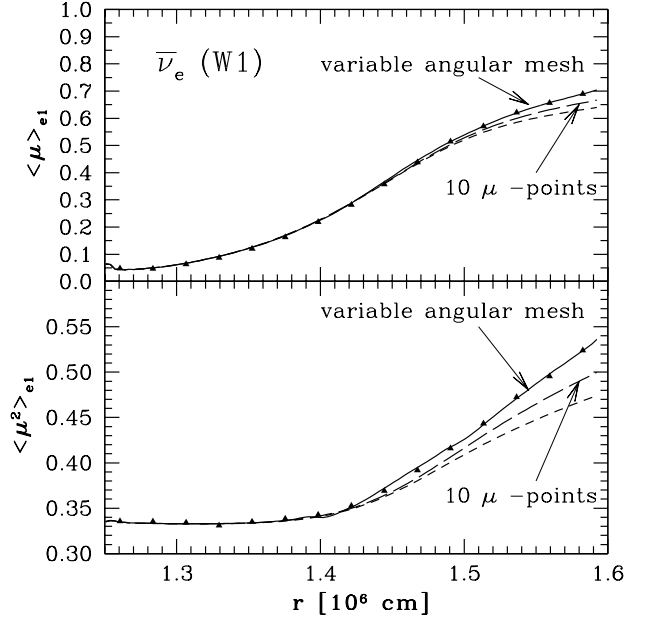


Fig. 10. The flux factors (upper panel) and the Eddington factor (lower panel) of the electron-type anti-neutrino for background model W1 with the long dashed lines for model FA where 10 angular mesh points are used instead of 6. The short dashed lines show for comparison the results of the corresponding standard model ST2. The solid lines are the result obtained with the variable angular mesh method. The Monte Carlo result is shown with the solid triangles.

this is why the inverse of the flux factor appears in Eq. (1)—the application of the Boltzmann solver with a relatively small number of angular mesh points may lead to an overestimation of the neutrino energy deposition in the hot bubble for disadvantageous situations, in particular when most of the heating occurs in those regions where the deviation of the flux factor from the correct value is significant. In contrast, all flux limiters used in MGFLD underestimate the heating rate significantly. Therefore, even for the Boltzmann solver, improvement of the angular resolution or a redistribution of the angular grid points is desirable in order to a priori avoid inaccurate evaluation of the heating rate. As already mentioned, an increase of the number of angular mesh points is not feasible. Choosing a variable angular mesh which adjusts mesh point locations in dependence of time and spatial position might be a solution. This issue will be discussed in the next subsection.

4.4. Variable angular mesh in the Boltzmann solver

Here we attempt to improve the angular resolution of the Boltzmann solver by redistributing the angular grid points

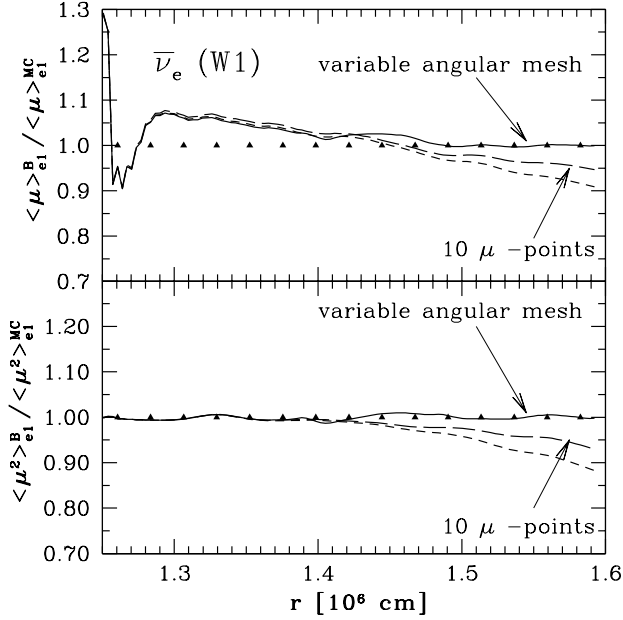


Fig. 11. Same as Fig. 10 but showing the ratios of the Boltzmann to the Monte Carlo results for the flux factor (upper panel) and the Eddington factor (lower panel). Again, the Boltzmann calculations with 6 angular bins (standard model ST2, short dashed lines), 10 angular bins (model FA, long dashed lines) and the variable angular mesh (solid lines) are shown. Between the radial grid points of the Monte Carlo simulation (whose locations are indicated by solid triangles), the Monte Carlo results are interpolated by cubic splines.

in dependence of time and position so that their density is enhanced in the forward direction in the optically thin region where the neutrino angular distribution becomes strongly forward peaked and the Boltzmann solver underestimates the flux factor and the Eddington factor. This requires adding extra angular advection terms in the numerical scheme which compensate for the motions of the angular mesh points.

We assume that the position of each interface of the angular grid is a function of time, baryonic mass and neutrino energy, i.e., $\mu_I = \mu_I(t, m, \varepsilon_\nu)$. Integrating Eq.(3) over angular bins then leads to the following additional angular advection fluxes at each angular mesh interface I :

$$-\frac{1}{c} \left(\frac{\partial \mu_I}{\partial t} \right) \left(\frac{f_\nu}{\rho_b} \right), \quad (21)$$

$$-4\pi\mu_I \left(\frac{\partial \mu_I}{\partial m} \right) e^\phi r^2 f_\nu, \quad (22)$$

$$-\left[\frac{1}{c} \frac{\partial (\ln \rho_b r^3)}{\partial t} \mu_I^2 - e^\phi 4\pi r^2 \rho_b \frac{\partial \phi}{\partial m} \mu_I \right]$$

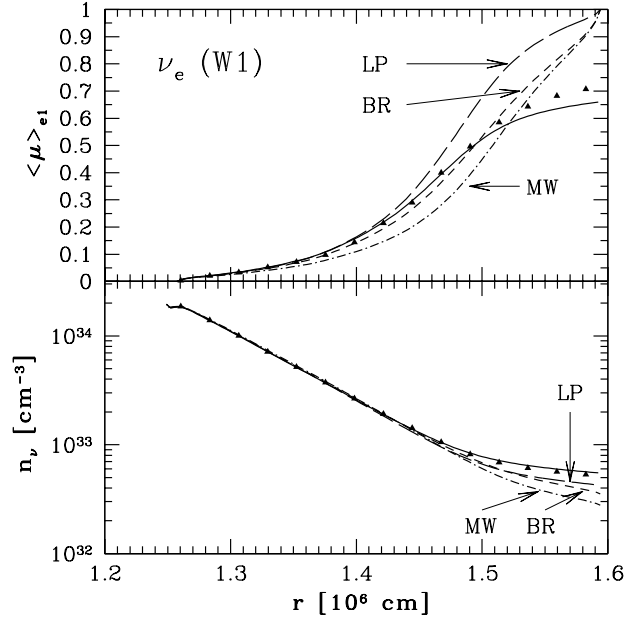


Fig. 12. The flux factors and number densities of the electron-type neutrino as obtained by MGFLD with three different flux limiters, Bruenn's (BR) with the short dashed lines, Levermore & Pomraning's (LP) with the long dashed lines, and Mayle & Wilson's (MW) with the dash-dotted lines. The background model is W1. For comparison, the Monte Carlo result and the Boltzmann result (model ST1) are also plotted with the triangles and the solid lines, respectively.

$$-\frac{1}{c} \frac{\partial (\ln r)}{\partial t} \left[\left(\frac{\partial \mu_I}{\partial \frac{1}{3}\varepsilon_\nu^3} \right) \left(\frac{f_\nu}{\rho_b} \right) \right]. \quad (23)$$

It is easy to understand that Eqs. (21)–(23) originate from the variability of the angular mesh points because of the differentials of the μ_I with respect to time, mass and neutrino energy.

Since the neutrino reaction rates are strongly energy dependent and so is the neutrino angular distribution, it would be desirable to implement the energy dependent angular mesh according to Eq. (23). In the current preliminary attempt, however, we installed only Eqs. (21) and (22) for simplicity. Incidentally, since Eq. (23) is proportional to $\frac{\partial \phi}{\partial m}$ in static background calculations, it is anyway negligible for the models considered here. We note that the motion of mesh points is not calculated implicitly, that is, the angular mesh points for the next time step are determined from the neutrino angular distribution at the current time step and are kept fixed during the implicit calculation of the transport for the next step.

In Fig. 10, we show both the flux factor and the Eddington factor obtained from the computation with the variable angular mesh. The improvement is clear from a

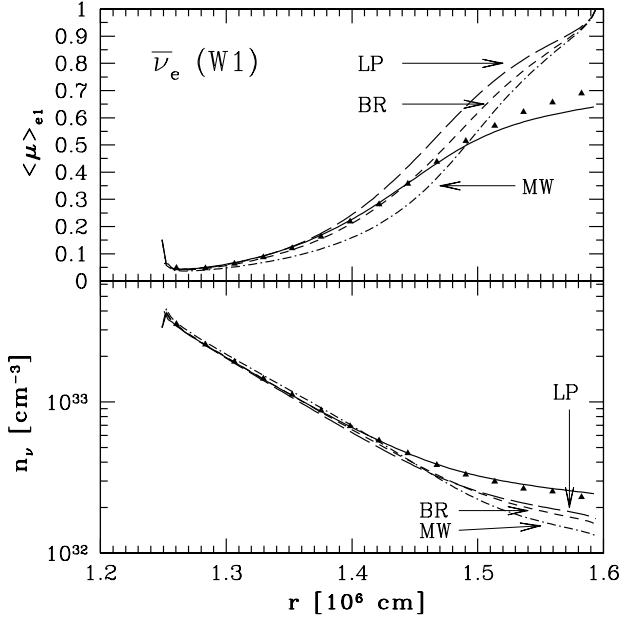


Fig. 13. The same as Fig. 12 but for the electron-type anti-neutrino.

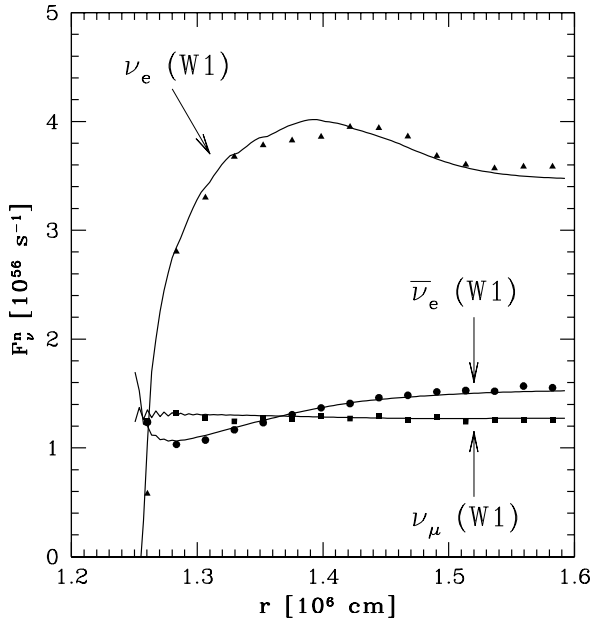


Fig. 14. The number fluxes of all types of neutrinos for background model W1. The filled symbols and the solid lines show the results of the Monte Carlo simulations and the Boltzmann simulations, respectively.

comparison with the result of model FA which employed 10 angular mesh points and is also shown in the figure. It should be emphasized that increasing the number of angular mesh points from 6 to 10 leads to an increase of CPU time by a factor of ~ 4.5 , while the additional operations for the variable angular mesh imply negligible computational load.

We repeated all Boltzmann calculations with the variable angular mesh method and found that the same improvement could be achieved for all cases. Our scheme is stable at least for the static background models, although the stability for dynamical background models remains to be tested. Thus we think this method is promising in applying the Boltzmann solver to the study of neutrino heating in the hot-bubble region of supernovae, although there is room for improvement concerning the prescription of the motion of the mesh points and the implementation of the energy-dependent angular mesh.

4.5. Spatial and energy resolution in the Boltzmann solver and radial advection

In this section we discuss how the numerical results change in dependence of the number of spatial and energy grid points, the boundary condition and the treatment of the radial advection in the Boltzmann solver.

In Fig. 15 we show the energy spectrum of electron-type anti-neutrinos for model FE, in which we used 18 energy mesh points, compared with the spectrum for the corresponding standard model ST2 which has 12 energy zones. No qualitative or quantitative difference is found between the two cases. This is also true for the luminosity and the angular distribution. Thus we think that about 15 energy mesh points are sufficient for the calculation of the energy spectrum. These results are in agreement with previous findings by Mezzacappa & Bruenn (1993a,b,c).

In models CS and NI we reduced the spatial resolution, because the Monte Carlo simulations were done with only 15 radial mesh points which were used to represent the stellar background on which the reaction kernels were evaluated. Another motivation for testing the sensitivity to the radial resolution is that it is hardly possible to describe the protoneutron star atmosphere with about 100 radial grid points in the context of a full supernova simulation. In model CS we used the same 15 spatial grid points as in the Monte Carlo simulations. On the other hand, in model NI we used 105 spatial mesh points but the density, temperature and electron fraction were not interpolated between the grid points of the Monte Carlo simulations.

In Fig. 16 we show the radial evolution of the average energy as defined in Eq. (9) and that of the number flux given by Eq. (19) for model CS, to be compared with the corresponding result for model ST2 in Fig. 14. It is clear that the agreement between the Monte Carlo and the Boltzmann results for both quantities is good.

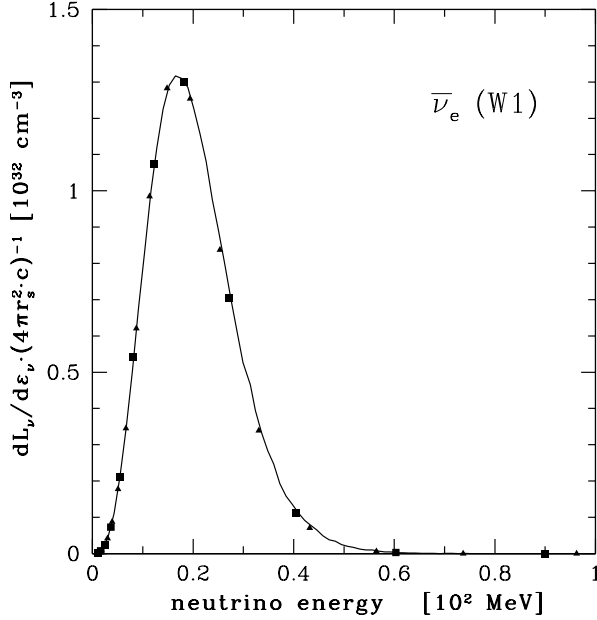


Fig. 15. The energy spectrum of electron-type anti-neutrinos calculated with 18 energy mesh points (model FE, filled triangles) for background model W1. The solid line shows the result of the Monte Carlo simulation, and the solid squares represent the result for the corresponding standard model ST2 with only 12 energy grid points.

We note also that the angular distribution as well as the energy spectrum are hardly affected by this change of the spatial resolution. Model NI agrees with the Monte Carlo data nearly perfectly (except for the problems with the angular distribution discussed in Sect. 4.3) after averaging over spatial mesh zones in accordance to the way the Monte Carlo data represent the transport result. Since the Boltzmann results do not change with the number of radial grid points, we conclude that the quality of the numerical solutions is not degraded very much for simulations with a decreased spatial resolution.

Minor oscillations of the number flux near the inner boundary can be seen in Fig. 14. This problem results from the fact that one cannot consistently specify the distribution of neutrinos which leave the computational volume at the inner boundary. While this distribution should be determined from the transport result just above the inner boundary, the Boltzmann solver, however, requires an ad hoc specification in order to calculate the flux at the inner boundary. This leads inevitably to an inconsistency of the flux in the innermost zone and thus to the observed oscillations. In fact, when an inhomogeneous spatial mesh was used in model NU, in which the innermost grid zone

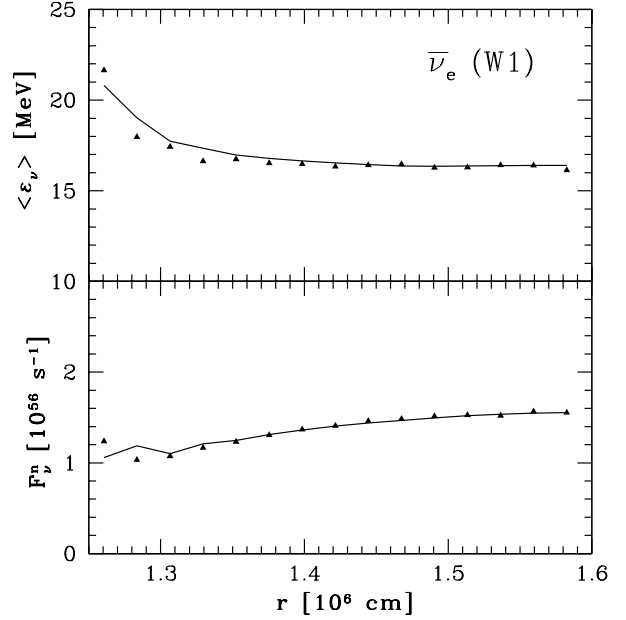


Fig. 16. The radial evolution of the average energy of the flux (upper panel) and the number flux (lower panel) of the electron-type anti-neutrino for model CS where 15 radial mesh points are used and the background model is W1. The filled triangles show the results of the Monte Carlo simulation, while the solid lines represent the results of the Boltzmann simulation.

was five times smaller than in the standard models, the oscillations were diminished as well.

Finally, we illustrate possible errors which are associated with the treatment of the finite differencing of the spatial advection term in the Boltzmann solver. In the radial advection term a linear average of the centered difference and of the upwind difference is used with a weight factor that changes according to the ratio of the neutrino mean free path to some chosen length scale. Mezzacappa et al. (1993a,b,c) took the ratio of the mean free path to the local mesh width in order to construct the weighting. However, we found that this does not work well if the mesh width becomes of the same order as the mean free path but is much smaller than the scale height of the background. This is indeed the case in the inner optically thick region of our standard models with 105 radial zones. In a more recent version of his code, Mezzacappa (private communication and 1998) defines the weighting factors by referring them to the neutrinospheric radius. In Fig. 17 the dashed line shows the number flux of muon-type neutrinos for model DI which used the prescription suggested by Mezzacappa et al. (1993a,b,c). The flux is slowly increasing with radius because the upwind differencing is given too large a contribution in the optically thick region where

the centered differencing should actually be chosen. As demonstrated by the solid line in Fig. 17, the constancy of the flux, however, is recovered when the ratio of the mean free path to the distance up to the surface is chosen instead of the ratio of the mean free path to the local mesh width. Yet, this issue is probably not very important for realistic calculations of the entire neutron star, since the mesh width is usually not much smaller than the typical scale height of the matter distribution.

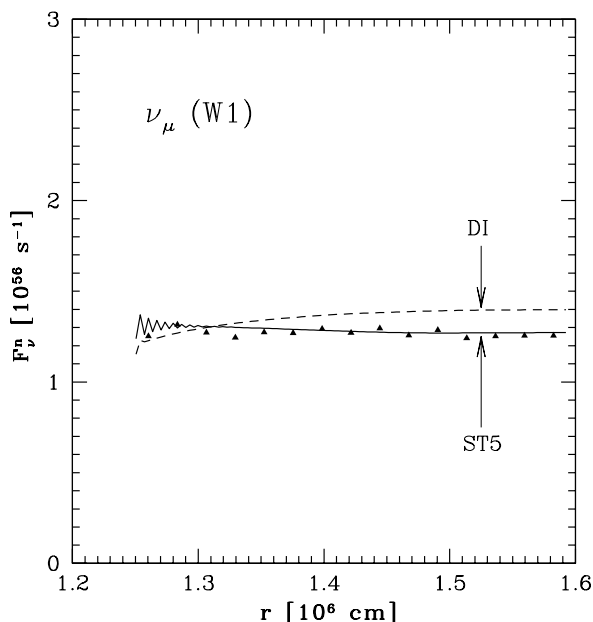


Fig. 17. The number fluxes of the muon-type neutrino for model DI (dashed line) and the corresponding standard model ST4 (solid line). The triangles are the result of the Monte Carlo simulation.

To finish, we comment briefly on a last model in which we assumed that the nucleon scattering is taken isotropic to see to what extent the result changes. No significant effect was found by modifying the angular distribution of the dominant scattering reaction.

5. Summary

In this paper an extensive comparison was made between a newly developed Boltzmann neutrino transport code based on the discrete ordinate (S_N) method as described by Mezzacappa & Bruenn (1993a,b,c), and a Monte Carlo transport treatment (Janka 1987, 1991a) by performing time-dependent calculations of neutrino transport through realistic, static profiles of protoneutron star atmospheres under the assumption of spherical symmetry. In particu-

lar, the sensitivity of the results of the Boltzmann solver to the employed numbers of radial, angular and energy grid points and to the treatment of the radial advection terms was investigated. The flux factor and Eddington factor, which contain information about the angular distribution of the neutrinos in the neutrino-decoupling region, were also compared with the approximate treatment of this regime by a multi-energy-group flux-limited diffusion code (MGFLD).

The Boltzmann and Monte Carlo results showed excellent agreement for observables such as the luminosity and the flux spectra which are determined in those regions of the star where the neutrino-matter interactions are still very frequent and thus the neutrino distributions are still nearly isotropic. Since the luminosity and the spectra are essentially conserved farther out, the spatial evolutions as well as the surface values exhibit this agreement, as long as the finite differencing of the Boltzmann solver is done in a conservative way.

Some problems, however, were observed concerning the description of the angular distribution of the neutrinos by the Boltzmann results in the semitransparent and transparent regimes. Due to severe limitations of the number of angular grid points which can be used—typically only 6–10 angular bins between zero and 180 degrees are compatible with the steep increase of the requirements of computer time for better resolution—the Boltzmann code is not able to describe strong forward peaking of the neutrino distributions very well, if a quadrature set is employed for the angular integration where the maximum angle cosine μ_{\max} is significantly less than unity. In this case the Boltzmann results *underestimate* the anisotropy in the optically thin region outside the average “neutrinosphere”, and the exact limits for the flux factor, $\langle \mu \rangle \rightarrow 1$, and for the Eddington factor, $\langle \mu^2 \rangle \rightarrow 1$, at large distances away from the neutrino source cannot be satisfactorily reproduced. This is in agreement with the trends also seen in recent results of Messer et al. (1998) and is exactly opposite to the deficiencies of MGFLD which tends to *overestimate* the radial beaming of the radiation because flux limiters enforce the free-streaming limit when the optical depth of the stellar background becomes very low (Janka 1991a, 1992).

Since the dominant energy deposition rate by absorption of electron neutrinos and antineutrinos in the hot-bubble region of the supernova core is inversely proportional to the flux factor (see Eq. (1)), which means that the energy transfer from neutrinos to the stellar plasma scales with the neutrino energy density (or number density) in the heating region, one cannot exclude that the Boltzmann solver may lead to an overestimation of the neutrino heating in disadvantageous situations, whereas MGFLD yields rates which are definitely too low. For a set of typical post-core bounce situations, Messer et al. (1998), however, claim on grounds of numerical tests that the net neutrino heating is converged with S_6 and that the differences between S_6 and S_4 are minor.

The problems may be more serious for neutrino reactions like neutrino-antineutrino annihilation which are sensitive to both the flux factor $\langle\mu\rangle$ and the Eddington factor $\langle\mu^2\rangle$ of the neutrinos (see Janka 1991b).

The description of the angular neutrino distribution by the Boltzmann solver and thus the agreement with the highly accurate Monte Carlo data can be significantly improved by employing a variable angular mesh, even without increasing the total number of angular mesh points. The positions of the angular grid points must be moved at each time step and in every spatial zone such that they are clustering in the forward direction in the optically thin regime.

We found that the energy spectra can be well calculated with about 15 energy mesh points. The fact that a reduction of the number of spatial grid points from more than 100 to only 15 in the neutron star atmosphere did not change the quality of the transport results means that the Boltzmann code can be reliably applied to realistic simulations which involve the whole supernova core. Moreover, it was demonstrated that the details of the interpolation between centered differencing and upwind differencing in the spatial advection term can affect the accuracy of the transport results.

The excellent overall agreement of the results obtained with the Boltzmann code and the Monte Carlo method confirms the reliability of both of them. Good performance of the S_N method for solving the Boltzmann equation of neutrino transport has been found before by Mezzacappa & Bruenn (1993a,b,c) and Messer et al. (1998) even for realistic dynamic situations. We hope that the work described here also helps to reveal possible deficiencies and weaknesses and thus will serve for further improvements of the numerical treatment of neutrino transport in supernovae and protoneutron stars.

Acknowledgements. Encouraging discussions and helpful suggestions by E. Müller are acknowledged. We are grateful to A. Mezzacappa for critical comments on a first version of the paper and for updating us with the most recent improvements of his code. This work was partially supported by the Japanese Society for the Promotion of Science (JSPS), Postdoctoral Fellowships for Research Abroad, and by the Supercomputer Projects (No.97-22 and No.98-35) of the High Energy Accelerator Research Organization (KEK). H.-T.J. was supported, in part, by the Deutsche Forschungsgemeinschaft under grant No. SFB-375. The numerical calculations were mainly done on the supercomputers of KEK.

References

- Bethe, H. A. and Wilson, J. R. 1985, *ApJ*, 295, 14
 Bionta, R. M. et al. 1987, *Phys. Rev. Lett.*, 58, 1494
 Bowers, R. L. and Wilson, J. R. 1982, *ApJS*, 50, 115
 Bruenn, S. W. 1985, *ApJS*, 58, 771
 Burrows, A. 1987, *ApJ*, 318, 57
 Burrows, A. 1997, to be published in the proceedings of the 18'th Texas Symposium on Relativistic Astrophysics, held in Chicago, 15 - 20 December 1996, edited by Olinto, A., Frieman, J. and Schramm, D., (World Scientific Press, Singapore, 1997)
 Burrows, A. and Goshy, J. 1993, *ApJ*, 416, 75
 Burrows, A., Hayes, J. and Fryxell, B. A. 1995, *ApJ*, 450, 830
 Burrows, A., Sawyer, R. F. 1998a, *Phys. Rev.*, C58, 554
 Burrows, A., Sawyer, R. F. 1998b, submitted to *Phys. Rev. Lett.*
 Cernohorsky, J. and Bludman, S. A. 1994, *ApJ*, 433, 250
 Dgani, R. and Janka, H.-Th. 1992, *A&A*, 256, 428
 Hannestad, S. and Raffelt, G. 1997, to appear in *ApJ*
 Herant, M., Benz, W., Hix, J., Freyer, C. and Colgate, S. A. 1994, *ApJ*, 435, 339
 Hillebrandt, W. and Wolff, R. G. 1985, *Nucleosynthesis : Challenges and New Developments*, edited by Arnett, W. D. and Truran, J. W., (University of Chicago press, Chicago, 1985), p131
 Hirata, K. et al. 1987, *Phys. Rev. Lett.*, 58, 1490
 Horowitz, C. J. and Wehrberger, K. 1991, *Phys. Lett. B*, 266, 236
 Janka, H.-Th. 1987, *Nuclear astrophysics; Proceedings of the Workshop, Tegernsee, Germany, Apr. 21.-24., 1987*, (Springer-Verlag, Berlin and New York, 1987), p319
 Janka, H.-Th. 1991a, Ph.D. thesis, Technische Universität München
 Janka, H.-Th. 1991b, *A&A*, 244, 378
 Janka, H.-Th. 1992, *A&A*, 256, 452
 Janka, H.-Th. 1993, *Frontier Objects in Astrophysics and Particle Physics, Proc. of the Vulcano Workshop 1992, Conf. Proc. Vol. 40*, edited by Giovannelli, F. and Mannocchi, G., (SIF, Bologna, 1993), p345
 Janka, H.-Th., Dgani, R. and van den Horn, L. J. 1992, *A&A*, 265, 345
 Janka, H.-Th. and Hillebrandt, W. 1989a, *A&AS*, 78, 375
 Janka, H.-Th. and Hillebrandt, W. 1989b, *A&A*, 224, 49
 Janka, H.-Th. and Keil, W. 1998, *Supernovae and Cosmology, Proc. of a Colloquium in Honor of Prof. G. Tammann on the Occasion of his 65th Birthday, Augst, Switzerland, Jun. 13., 1997*, edited by Labhardt, L., Binggeli, B. and Buser R., (Astronomisches Institut der Universität Basel, Basel, 1998) p7
 Janka, H.-Th., Keil, W., Raffelt, G. and Seckel, D. 1996, *Phys. Rev. Lett.*, 76, 2621
 Janka, H.-Th. and Müller, E. 1993, *Frontiers of Neutrino Astrophysics, Proc. of the International Symposium on Neutrino Astrophysics, Takayama/Kamioka, Japan, Oct. 19.-22., 1992*, edited by Suzuki, Y. and Nakamura, K., (Universal Academy Press, Tokyo, 1993) p203
 Janka, H.-Th. and Müller, E. 1996, *A&A*, 306, 167
 Keil, W., Janka, H.-Th. and Müller, E. 1996, *ApJ Lett.*, 473, L111
 Keil, W., Janka, H.-Th. and Raffelt, G. 1995, *Phys. Rev.*, D51, 6635
 Lichtenstadt, I., Khokhlov, A. M. and Wheeler, J. C. 1998, submitted to *ApJ*
 Mayle, R. and Wilson, J. R. 1988, *ApJ*, 334, 909
 Messer, O. E. B., Mezzacappa, A., Bruenn, S. W. and Guidry, M. W. 1998, submitted to *ApJ*, astro-ph 9805276
 Mezzacappa, A. 1998, *J. Computational and Applied Mathematics*, in press
 Mezzacappa, A. and Matzner, R. A. 1989, *ApJ*, 343, 853

- Mezzacappa, A. and Bruenn, S. W. 1993a, *ApJ*, 405, 637
Mezzacappa, A. and Bruenn, S. W. 1993b, *ApJ*, 405, 669
Mezzacappa, A. and Bruenn, S. W. 1993c, *ApJ*, 410, 740
Mezzacappa, A. et al. 1998, *ApJ*, 495, 911
Miller, D. S., Wilson, J. R. and Mayle, R. W. 1993, *ApJ*, 415, 278
Misner, C. W. and Sharp, D. H. 1964, *Phys. Rev.*, 136, B571
Myra, E. S. et al. 1987, *ApJ*, 318, 744
Prakash, M. et al. 1997, *Phys. Rep.*, 280, 1
Raffelt, G. G. and Seckel, D. 1995, *Phys. Rev.*, D52, 1780
Raffelt, G. G., Seckel, D. and Sigl, G. 1996, *Phys. Rev.*, D54, 2784
Reddy, S., Prakash, M. and Lattimer, J. M. 1997, *ApJ*, 478, 689
Reddy, S., Prakash, M. and Lattimer, J. M. 1998a, to appear in *Proc. Second Oak Ridge Symposium on Nuclear and Atomic and Nuclear Astrophysics*
Reddy, S., Prakash, M. and Lattimer, J. M. 1998b, *Phys. Rev.*, D58, 1309
Sawyer, R. F. 1989, *Phys. Rev.*, C40, 865
Schinder, P. J. 1990, *ApJS*, 74, 249
Shimizu, T., Yamada, S. and Sato, K. 1994, *ApJ Lett.*, 432, L119
Smit, J. M., Cernohorsky, J. and Dullemond, C. P. 1997, *A&A*, 325, 203
Sumiyoshi, K. and Ebisuzaki, T. 1998, *Parallel Computing*, 24, 287
Suzuki, H. 1990, Ph.D. Thesis, University of Tokyo
Suzuki, H. 1993, *Frontiers of Neutrino Astrophysics*, *Proc. of the International Symposium on Neutrino Astrophysics, Takayama/Kamioka, Japan, Oct. 19.–22., 1992*, edited by Suzuki, Y. and Nakamura, K., (Universal Academy Press, Tokyo, 1993) p219
Suzuki, H. 1994, *Physics and Astrophysics of Neutrinos*, edited by Fukugita, M. and Suzuki, A., (Springer-Verlag, Tokyo, 1994), p763
Tubbs, D. L. 1978, *ApJS*, 37, 287
Tubbs, D. L. and Schramm, D. N. 1975, *ApJ*, 201, 467
Wilson, J. R. 1982, *Proc. Univ. Illinois Meeting on Numerical Astrophysics*
Wilson, J. R. 1988, private communication
Wilson, J. R. and Mayle, R. W. 1988, *Phys. Rep.* 163, 63
Wilson, J. R. and Mayle, R. W. 1993, *Phys. Rep.* 227, 97
Wilson, J. R., Mayle, R. W., Woosley, S. E. and Weaver, T. 1986, *Ann. N. Y. Acad. Sci.*, 470, 267
Yamada, S. 1997, *ApJ*, 475, 720